J. Eng. Technol. Sci., Vol. 54, No. 2, 2022, 220201

The Potential of Corncobs in Producing Reduced Graphene Oxide as a Semiconductor Material

Kusuma Wardhani Mas'udah[1,2,*], Ahmad Taufiq[3] & Sunaryono[3]

[1]Faculty of Science and Technology, University of Pesantren Tinggi Darul Ulum, PP. Darul 'Ulum Tromol Pos 10 Peterongan Jombang 61481, Indonesia
[2]Department of Mechanical Engineering, Faculty of Engineering, University of Pembangunan Nasional 'Veteran' Jawa Timur, Jalan Rungkut Madya No. 1 Surabaya 60294, Indonesia
[3]Department of Physics, Faculty of Mathematics and Natural Sciences, Universitas Negeri Malang, Jalan Semarang 5 Malang 65145, Indonesia
*E-mail: kusuma.w.fisika@upnjatim.ac.id

Highlights:

- The development of carbon material (reduced graphene oxide/RGO) from biomass (corncobs), which can be utilized as a renewable technology.
- Corncobs were used to produce RGO using the acid-base method.
- The addition of PEG-2000 in synthesizing RGO brings out its unique characteristics, especially its functional groups.

Abstract. A simple chemical approach was developed to synthesize reduced graphene oxide (RGO) from corncob waste through the acid-base method with the addition of PEG-2000 at specific concentrations. The morphology and structure of RGO were characterized by scanning electron microscopy and energy-dispersive X-ray spectroscopy. The process of reduction and quality of RGO were examined carefully with UV-Vis spectroscopy, infrared spectroscopy, and X-ray diffractometry. Based on the treatment and characterization, the diffraction data showed a prominent peak of RGO at a 2-theta position of 24.01°. The existence of C=C functional groups was detected in aromatic compound groups and alkene functional groups in aliphatic hydrocarbon compounds by infrared spectroscopy. The use of corncobs as the main raw material synthesized by an environmentally friendly route has tremendous potential in producing RGO that can be used as an efficient semiconductor material.

Keywords: *absorbance; band gap energy; corncob; phase structure; RGO.*

1 Introduction

In recent times, graphene has attracted much attention because of its excellent properties, such as ultrafast electron transport [1,2], high specific surface area [3], high adsorption rate [4,5], high mechanical strength, chemical, and thermal

Received July 4th, 2020, 1st Revision December 2020, 2nd Revision August 6th, 2021, Accepted for publication August 31st, 2021.
 ISSN: 2337-5779, DOI: 10.5614/j.eng.technol.sci.2022.54.2.1

stability [6]. In relation to the specific properties of graphene, especially as a two-dimensional nanomaterial with a greater number of site traps, graphene holds promise as a semiconductor material with great strength. The conjugated electronic structure π at the atomic scale of graphene makes it the main electron receiver. Graphene transfers electrons it receives very quickly and easily because of its zero-band structure [7]. Graphene is a layered arrangement (with 2 or 3 layers) of hexagon carbon in the form of sheets (2 dimensions), like a thin sheet of paper that can easily be wrinkled but is quite strong [8].

It has been proven that graphene has a number of special characteristics, including strong optical properties [9], high thermal conductivity up to 5000 $W.m^{-1}.K^{-1}$ [10], high electrical conductivity of 21 $S.m^{-1}$ [11], and high strength with a power density of 2353 $W.kg^{-1}$ [12]. Another outstanding characteristic of graphene is its high specific surface area up to 2675 $m^2.g^{-1}$ [13]. A number of oxygen (O) atoms can be inserted into the carbon bonds to form graphene oxide compounds. The graphene oxide can be reduced so that the oxygen atoms are reduced and leave a defect in the form of a loose carbon bond, where the honeycomb shape undergoes a change (distortion) and other defects, thus forming reduced graphene oxide (RGO). In general, it consists of three main peaks, namely C-C/C=C at 284.4 eV, C-O at 286.4 eV, and C=O at 288.1 eV, and has a specific capacitance of 350.3 $F.g^{-1}$ [14].

Graphene and its derivatives (GO and RGO) are now being developed very intensively for various applications [15,16]. Graphene, which is also widely developed by many experts, is a semiconductor material. Gao, *et al.* [17] have presented the use of single-layer graphene as electrode for the development of a new electronic device that exploits the unique structure of thin atomic matter. Furthermore, graphene can also function as photocatalytic compound [7,18] to eliminate contamination [19], H_2 evolution [20], and CO_2 reduction [21]. Interestingly, Huang, *et al*. reported that the addition of PEG into RGO could increase its tensile strength up to 59.46 MPa and its conductivity up to 9.69×10^{-4} $S.cm^{-1}$ [22]. Moreover, Li, *et al*. [23] reported that the addition of PEG into RGO could increase its thermal conductivity by 51.79 (152.46%) with a high-energy storage density of 131.94 $J.g^{-1}$.

Graphene, aside from containing main carbon-based components, can also be produced using natural resources, such as biomass waste from corncobs. The amount of biomass waste generated from agricultural production activities is abundant, especially in Indonesia. Corn as a source of renewable energy is not extensively utilized in Indonesia. Based on the current data, it is estimated that the amount of corncob waste produced in Indonesia is around 5.7 million tons per year. The corncobs waste tends to be thrown away and burned, causing pollution problems and exacerbating the greenhouse effect and global warming [24].

Therefore, it is important to develop corncob waste to increase its scientific and economic value for human life, for example as semiconductor material. Semiconductors have a resistivity between the conductor and the insulator of around 10^{-2} to 10^{-9} Ω.m. The bandgap energy (Eg) in semiconductors is much smaller than in insulators and causes semiconductors to have different behavior from insulators [25]. Semiconductors are materials with a valence band that is almost full while the conduction band is almost empty with an Eg value of 1 to 2 eV) [26].

In the last few years, several researchers have intensively focused on RGO production. However, cost-effectiveness improvement in large-scale production of RGO still has to be studied more deeply, especially regarding the raw materials and method development. RGO synthesized from biomass materials such as coconut shells has a maximum bandgap of 1.87 eV [27]. Our previous research successfully developed a corncob pretreatment to produce RGO [8]. However, optimization of the production of high purity RGO from corncob waste with various treatments is important to be conducted. To produce high purity RGO from corncob waste, the washing treatment using the acid-base method and various additions of PEG are essential factors to be calculated [23,28]. Furthermore, despite the detailed structure, the electrical properties as well as the energy band gap [29] are also important to be taken into account. The addition of PEG into RGO can enhance its thermal conductivity and the efficiency of the storage energy performance. In addition, well-distributed PEG in RGO acts as a heat transfer medium and reduces the thermal resistance of the interface for thermal energy transfer between RGO and PEG during the thermal energy storage/release process [23]. Our investigation of the influence of PEG on the structural and electrical characteristics of RGO is reported in this paper.

2 Materials and Methods

To obtain corncob powder, corncobs that had been cleaned from corn grains were dried at 100 °C. The corncobs were then crushed to form a fine powder and filtered using filter paper of 200 mesh. Further, the corncobs were washed using the acid-base method to remove impurities in the sample to obtain RGO. This was done by mixing 10 g of corncob powder with 80 mL of HCl. The mixture was stirred using a magnetic stirrer at a speed of 750 rpm at room temperature for 20 min. Titration was then carried out adding 80 mL of NH_4OH solution into the mixture with stirring at a speed of 720 rpm at room temperature for 30 min. The resulting product was washed using distilled water up to pH 7 to obtain a precipitate. The precipitate was then heated in an oven at 100 °C to obtain powder samples [8].

In the following step, the RGO powder was mixed with PEG-2000. In this stage, 1 g of PEG 2000 was mixed with 40 mL of distilled water at a temperature of 90 °C using a magnetic stirrer at 700 rpm rotation. The process of stirring was carried out for 30 min. Afterward, 20 mL of PEG-2000 solution was mixed with 3 g of RGO powder and stirred for 1 h at 750 rpm. This process was intended to homogenize the mixture evenly so that no aggregation occurred. The precipitate obtained from the filtering process was dried at 100 °C for 5 h until it became powder [30].

The RGO powder phase obtained after the washing process and mixing with PEG-2000 was evaluated using X-ray diffraction (XRD) at a 2-theta (2θ) position of 10° to 50° with a step size of 0.02°. The XRD used a radiation source of K-α_1 (1.5046 Å) and K-α_2 (1.5444 Å). The composition of chemical elements in the corncob powder was determined by energy-dispersive X-ray (EDX) analysis. The phase identification process was based on matching the diffraction pattern data to a reference database. Analysis of the functional groups was done using Fourier transform infrared spectroscopy (FTIR). The wavelength range used was between 500 cm^{-1} and 4000 cm^{-1}. Furthermore, a UV-Vis spectrophotometric test was performed to determine the bandgap. The measurement was maintained in the wavelength range of 190 to 1100 nm and its data analysis related to the relationship between reflectance and absorbance was as follows:

$$A = log_{10}(\frac{1}{R}) \qquad \text{(for \%R)} \qquad (1)$$

The relationship between absorbance and transmittance is:

$$A = 2 - log_{10}\%T \qquad (2)$$

Tauc's relation [31] is as follows:

$$Ahv = B(hv - Eg)^{\gamma} \qquad (3)$$

where:

A = Absorbance
Eg = Bandgap energy
h = Planck's constant around 6.626×10^{-34} J.s or 4.14125×10^{15} Ev.s ($1\ eV = 1.6 \times 10^{-19}$ J)
v = Frequency (equivalent to $c.\lambda^{-1}$; where $c = 3 \times 10^{8}$ $m.s^{-1}$, and
λ = Wavelength obtained in nm)
γ = ½ for direct type and 2 for indirect type
B = An energy-independent constant sometimes called the band tailing parameter [32]

Generally, the Eg of the RGO-PEG is calculated by plotting $(\alpha hv)^2$ versus photon energy (hv) using the data obtained from the optical absorption spectra.

3 Results and Discussion

3.1.1 SEM Analysis

SEM images of the corncobs, the RGO, and the RGO-PEG powders are shown in Figure 1. The structures of the corncobs (Figure 1a), RGO (Figure 1b), and RGO-PEG (Figure 1(c)) were clearly revealed by the SEM investigation. The corncob powder had a porous surface structure covered with a structure of impurities (Figure 1(a)) [19,33]. Compared to the SEM results of the corncob powder, the SEM micrographs of the RGO powder that resulted from the acid-base treatment mostly had a flat structure (Figure 1b). Meanwhile, due to the mixing of RGO and PEG a large porous structure is formed, as can be seen in Figure 1c. It is possible that RGO, which has a flattened structure, adheres to the PEG and exists as a pore enveloping layer, indicating that the PEG completely covers the support material [23]. The average size of RGO attached to the PEG surface was 422.5 nm and the average pore size was 1.1 µm.

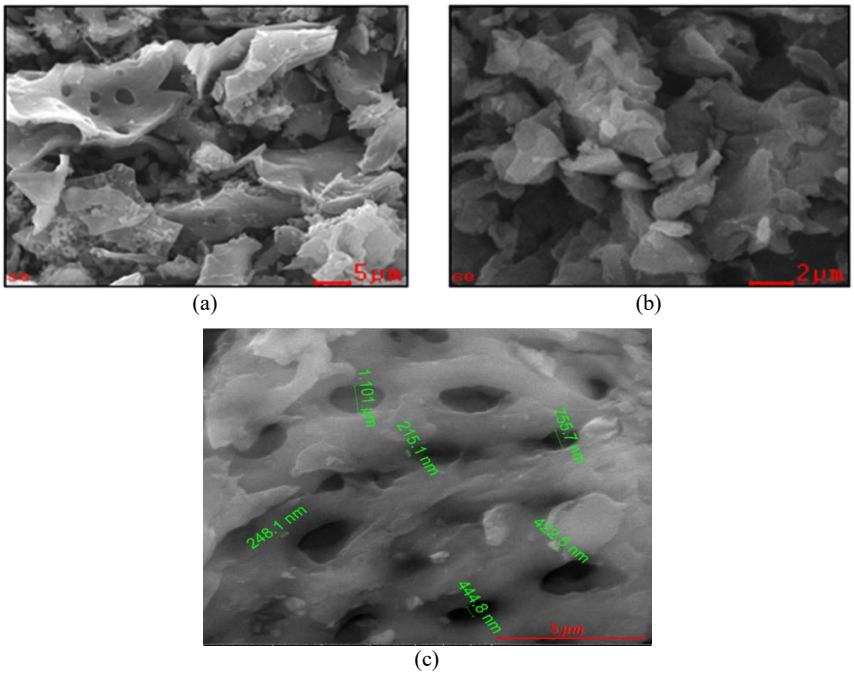

(a) (b)

(c)

Figure 1 SEM images of (a) corncob powder, (b) RGO powder, and (c) RGO-PEG powder.

3.1.2 Elemental Composition Analysis Using EDX

Examination of the chemical composition of the samples was carried out to determine which elements were contained in the corncob powder as raw organic material. The organic material is naturally abandoned and has a fairly high impurity level. Impurities can be removed by several treatments, such as heating at a certain temperature according to the elements of impurity contained in it [8]. The corncob powder contained the element carbon (C) at a percentage of 71.11%. Other elements contained in the corncob powder were oxygen (O), magnesium (Mg), aluminum (Al), silicon (Si), phosphorous (P), potassium (K), and calcium (Ca), as shown in Table 1.

The elements of impurity formed crystalline peaks, as shown by the XRD characterization results (Figure 3). The presence of metal elements in the corncobs could be originated from the type of soil at the time of planting. In its growth, the corn tree needs nutrients found in the soil. These nutrients consist of two types, namely macronutrients and micronutrients.

Macronutrient elements are C, H, O, N, P, K, Ca, Mg, and S, while micronutrient elements are Fe, Mn, B, Cu, Zn, Cl, and Mo. Some of these elements come from the air and some come from the ground [34]. Elements contained in the soil can be absorbed by the corn tree through the roots of the corn tree, which can be distributed during growth to all parts of the tree, including the corncobs, so that the corncobs contain some of these metal elements. The atomic percentage values of these elements are shown in Table 1. The high contents of carbon and oxygen in the corncob powder could be used as a reference indicating that there are structures and phases of either graphene, graphene oxide, reduced graphene oxide, or graphite by providing a heating treatment (Figure 2) [35].

Table 1 Elemental composition of the samples.

Element	Sample a (%)	Sample b (%)
C	71.11	78.83
O	22.30	20.27
Mg	00.70	-
Al	00.54	00.30
Si	01.44	00.59
P	00.60	-
K	01.69	-
Ca	01.62	-

The RGO powder washed using the acid-base method was able to reduce metal elements such as Mg, P, and K. Al and Si still appeared but at a percentage below 1%. In Table 1 it appears that the increase in the percentage of carbon atoms in sample b was 78.83%. This is because washing with the acid-base method can

remove the impurity phase in corncob powder when dissolved into hydrochloric acid to obtain RGO powder [36]. Furthermore, in the RGO, after mixing in the PEG-2000, the remaining elements were C, O, and Si. The percentage of carbon increased drastically by 90.19%. The addition of PEG-2000 into the RGO powder was not able to reduce the Si in the sample even though the percentage was very small because PEG-2000 is able to bind Si [23].

3.1.3 Analysis of X-Ray Diffraction

The phase change behavior of the corncob powder, the RGO powder, and the RGO-PEG was measured using XRD, as shown in Figures 3(a-c). XRD characterization was carried out to determine the crystal structure by maintaining 2-theta at 5° to 55°. The diffraction patterns produced by the corncob powder consisted of a wide peak located around a 2-theta position of 18.47° to 35° (Figure 3(a)) and also impurity peaks with high intensity. The impurity peaks can be removed by washing with the acid-base method. The diffraction patterns of the washed RGO powder sample are shown in Figures 3b and 3c for RGO-PEG 2000 (Figure 3(c)).

The figures show one large peak in the range of 16° to 30° for 2-theta. The wide peak of corncob powder had a lower peak intensity compared to the RGO and RGO-PEG 2000 powders. This phenomenon can be attributed to the more serious inhibitory effect of the carrier micropore structure on the thermal diffusion motion of the PEG molecular segments [23]. Moreover, compared to RGO-PEG 2000, the slightly higher temperature used during the PEG dissolution process against RGO could be attributed to the nucleation sites provided by the porous support for PEG crystallization during the solidification process, which accelerated the crystallization of the RGO-PEG 2000.

Figure 2 indicates the RGO phase, a graphite constituent layer that is still arranged randomly and undirected, producing an amorphous structure commonly referred to as a turbostratic structure [35]. The increase in intensity along with the addition of the treatment applied to the RGO-PEG 2000 indicates an additional regularity of the layer arrangement of hexagonal carbon atoms (sp^2), arranged so that it becomes an amorphous graphite structure that is like a turbostratic structure [37]. Based on our observations, Figures 3(b) and 3(c) show that two peaks piled together to form a large camel hump. In Figure 3(b), the highest peak is the second peak, located at an angle of 24.01°. In Figure 3(c), the highest peak is the first peak, located at an angle of 21.85°. The camel hump-like peak width in both samples b and c above indicates the presence of several oxygen functional groups remaining in the sample, so that they are included in the prepared corncob graphene oxide group.

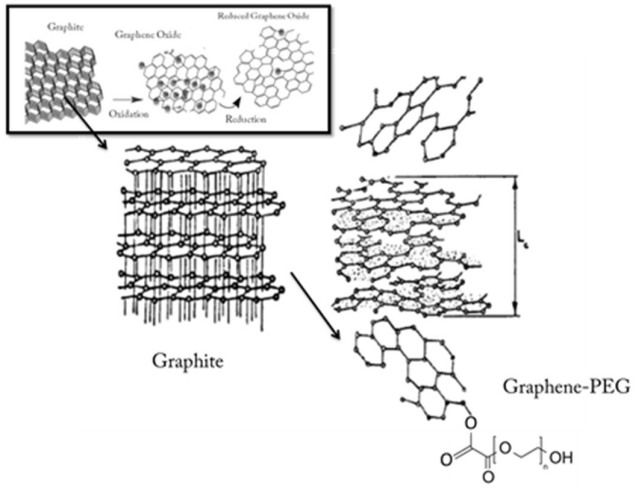

Figure 2 Formation of PEG-modified RGO-PEG [35].

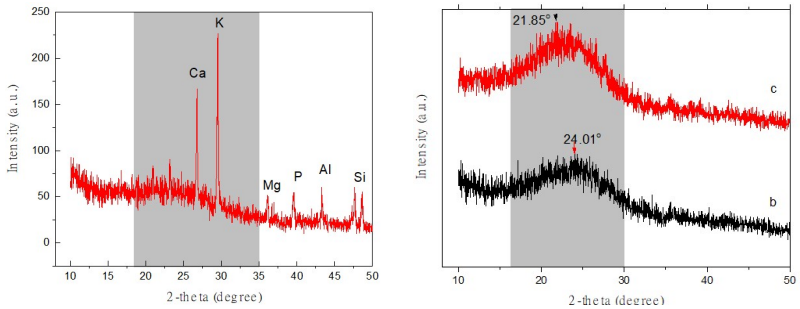

Figure 3 XRD patterns: (a) corncob powder, (b) RGO powder, and (c) RGO-PEG powder.

Based on the observed peak expansion, it was concluded that the graphene build-up was poorly ordered, which is called reduced graphene oxide [38]. This is also supported by the results of the characterization tests using FTIR. In the RGO powder that was washed using the acid-base method, it was indicated that RGO phase was formed, which is supported by the results of the FTIR graphic pattern in Figure 4. The number of bonds formed between C=O, CO, C=C, and O-H indicates that RGO phase was formed. In line with this work, the previous work [35] showed that RGO could be formed at low temperature, i.e., 100 °C. At low temperatures, there are still many hydroxyl (O-H) bonds, carbonyl (C=O), and aromatic (C-H) bonds. The wide peak pattern formed at a 2-theta position of 23° indicates RGO phase with reflection from plane (002) in the graphite amorphous

carbon structure [39]. The resulting wide peak indicates a small crystallite size of the RGO phase. The wide peak indicates that the RGO seam structure is structured in a short span of piles.

3.1.4 Analysis of Infrared Spectroscopy

The functional groups in a compound in organic or inorganic materials can be identified using FTIR. FTIR is a spectroscopic device that uses the Fourier transform method to measure the infiltration of the infrared spectrum emitted from the source to the test a material at various wavenumbers. The output obtained from FTIR spectroscopy is in the form of a graph of the peaks of the interactions of each molecule in the test material absorbing energy from the infrared spectrum shown by a graph of the relationship of the transmission and the wavenumber (cm^{-1}). Each of the bonding molecular atoms has its respective energy absorption spectrum [40].

The results of the graph of the infrared spectra of the absorption results for the initial corncob powder are shown in Figure 4. The FTIR spectra of corncob powder show the main bonds, namely the functional group C=C alkynes at wavenumbers of 2139.06 cm^{-1} and 2220.07 cm^{-1}. The majority of the carbon is in the corncob powder; the double bond is the main structure in the corncob powder among other atomic bonds [41], and a peak appears at wave number 470.63 cm^{-1}, which probably indicates the presence of a C-H (bending) functional group [37]. The next three peaks, which are the out-of-plane bending bonds of C-H, are at wavenumbers of 759.95, 800.46, and 875.68 cm^{-1}. The outward bending bond vibration of = C-H is included in the alkene functional group with a wavenumber range of 600 to 1000 cm^{-1} [42]. Sharp and pointed peaks are then owned by four peaks, which are bond strains from C-O. C-O bond strain vibrations of functional groups of alcohols and phenols are in the range of 1000 to 1300 cm^{-1} [39]. The C-O bond strain found in the corncob powder was located at wavenumber 1049.28 cm^{-1}.

The next peak was at wavenumbers of 2843.07, 2873.94, and 2953.02 cm^{-1}, owned by C-H methylene asymmetric bond strain vibrations. The peak had a moderate transmission percentage and was not too sharp. The final peak, resulting from infrared spectrum radiation to the corncob powder, shows bond strain vibrations of O-H, which is a hydroxyl functional group. The peak of the O-H bond had a deeper and wider transmittance value compared to the other bond peaks, which shows the absorption energy of the infrared spectrum of a large sample [39].

Figures 4b and 4c show that the results of the infrared spectrum of the two types of treatment produced almost the same peak position pattern. The only difference

is in the transmission intensity percentage absorbed by each molecular bond contained in the old corncob powder. The difference in the value of the percentage of transmission intensity of these three samples is because each molecular bond held by each corncob absorbs a different amount of infrared spectrum energy, according to the vibrations of the atoms that occur during energy absorption throughout the entire range of wavenumbers. The absence of absorption by a compound at a particular wavenumber detected is called the baseline. Meanwhile, if a compound absorbs radiation at a particular wavenumber, the intensity of the radiation spectrum transmitted to the material will decrease. This results in a decrease in transmittance and appears in the spectrum pattern as a well (dip), called an absorption peak [40].

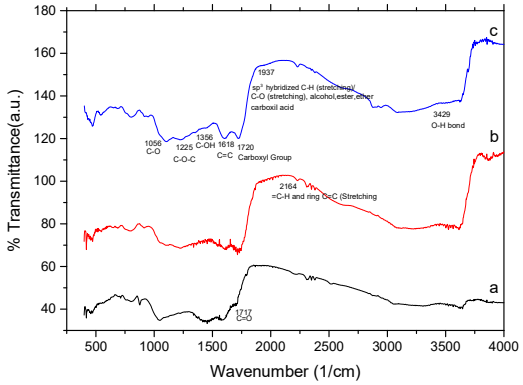

Figure 4 FTIR spectra of (a) corncob powder, (b) RGO powder, and (c) RGO-PEG powder.

Table 2 FTIR results of corncob powder.

Peak	Intensity	Corr. Intensity	Base (H)	Base (L)	Area	Corr. Area	Functional Groups
470.63	38.167	1.387	497.63	464.84	13.201	0.221	C-H (Bending)
759.95	44.271	0.581	769.6	727.16	14.669	0.142	C-H Alkene
800.46	43.531	0.324	810.1	771.53	13.798	0.06	C-H Alkene
875.68	41.978	3.264	894.97	854.47	14.473	0.549	C-H Alkene
1049.28	34.72	3.109	1080.14	929.69	62.353	2.866	C-O
2139.06	58.164	0.047	2140.99	2094.69	10.754	0.008	C=C Alkuna
2220.07	56.317	0.084	2222	2142.91	19.226	0.093	C=C Alkuna
2310.72	53.84	0.356	2314.58	2254.79	15.265	0.026	CO_2 Background FTIR
2517.1	51.784	0.142	2520.96	2447.67	20.244	0.03	O-H Carboxylic Acid
2586.54	51.395	0.036	2588.47	2540.25	13.794	0.007	O-H Carboxylic Acid
2679.13	50.212	0.058	2681.05	2642.48	11.417	0.002	O-H Carboxylic Acid
2843.07	47.271	0.151	2846.93	2733.13	35.908	0.031	C-H
2873.94	46.32	0.266	2879.72	2848.86	10.182	0.042	C-H Alkanes
2953.02	45.178	0.158	2956.87	2920.23	12.479	0.058	C-H Alkanes
3614.6	40.437	0.576	3618.46	3589.53	11.196	0.06	O-H Alcohol Monomer

Table 3 FTIR results of RGO powder washed using the acid-base method.

Peak	Intensity	Corr. Intensity	Base (H)	Base (L)	Area	Corr. Area	Functional Groups
688.59	37.341	0.801	713.66	675.09	16.278	0.171	C-H Alkene
746.45	37.057	0.133	748.38	725.23	9.768	0.018	C-H Alkene
914.26	37.509	1.054	933.55	875.68	24.19	0.401	C-H Alkene
1056.99	30.467	0.159	1058.92	952.84	48.884	0.185	C-O Alcohol
1099.43	29.335	0.103	1101.35	1058.92	22.203	0.014	C-O Alcohol
1176.58	28.807	0.056	1178.51	1141.86	19.553	0.013	C-O Alcohol
1219.01	28.066	0.079	1220.94	1178.51	23.169	0.024	C-O Alcohol
1317.38	29.391	0.51	1330.88	1309.67	11.156	0.051	C-O-C
1593.20	27.886	0.44	1597.06	1577.77	10.522	0.08	C=C aromatic ring
2229.71	59.689	1.158	2249	2189.21	13.028	0.228	C=C
2310.72	56.659	0.604	2314.58	2250.93	14.496	0.036	CO_2 Background FTIR
2600.04	48.496	0.071	2601.97	2389.8	60.449	0.712	O-H Carboxylic Acid
2839.22	44.887	0.333	2848.86	2704.2	48.509	0.255	C-H
2910.58	43.159	0.375	2916.37	2850.79	23.468	0.23	C-H Alkanes
2953.02	41.843	0.2	2956.87	2918.3	14.327	0.065	C-H Alkanes
3064.89	37.808	0.271	3068.75	3037.89	12.792	0.045	C-H Aromatic
3361.93	37.862	0.457	3373.5	3350.35	9.715	0.067	Hydrogen bonding alcohol

The next three peaks in the successive fingerprint region were at wavenumbers 688.59, 746.45, and 914.26 cm^{-1}, i.e. in the range of wavenumbers 600 to 1000 cm^{-1} owned by out-of-plane bending of C-H bonds in aromatic compounds [39]. One of the C-H bonds included in the aromatic compound shows that this carbon is a double bond with another atom and is a single covalent bond with hydrogen, which is part of substitution in the structure of benzene. Besides, one characteristic of organic material in addition to the presence of carbon and oxygen is the presence of hydrogen atoms [37]. The next peak occurs in the wavenumber range 1000-1300 cm^{-1}, which is included in the C-O bond strains of alcohol and phenol functional groups. The C-O bond strains are shown by the peaks at wavenumbers 1056.99, 1099.43, 1176.58, and 1219.01 cm^{-1} and other oxygen bridges, such as C-O-C, C-O-H, and C-O at wavenumbers 1020 to1463 cm^{-1} [43]. The bond strain C=C belongs to the range of wavenumbers 1430 to 1680 cm^{-1}. C=C bond strains in this range of wave numbers belong to the group of aromatic compounds and alkene functional groups in aliphatic hydrocarbon compounds [34]. In comparison, the C=C bond strain at wavenumbers 2100 to 2260 cm^{-1} probably indicate the presence of a C=C alkuna functional group. The existence of C=C bond strain is visible at wavenumbers 1593.20 and 2229.71 cm^{-1}.

The FTIR spectrum of RGO-PEG in Figure 3c has a broad peak at 3429 cm^{-1} in the high-frequency region associated with the O-H bonding stretching mode, which indicates the presence of hydroxyl groups in RGO [43]. The peak at a wavenumber of 1937 cm^{-1} probably indicates the presence of sp3 hybridization C-H (strain)/C-O (stretching), alcohol, esters, ether, and carboxylic acid [37]. The peak at a wavenumber of 1720 cm^{-1} probably indicates the presence of a carboxyl group. The sharp peak found at a wavenumber of 1615 cm^{-1} is a resonance peak

that can be set for vibration stretching and bending OH molecules of water molecules adsorbed on graphene oxide. The peak at a wavenumber of 1356 cm^{-1} arises from the C-OH group. The peak at 1225 cm^{-1} indicates the stretching of C-O-C and the peak at a wavenumber of 1056 cm^{-1} probably indicates the vibration mode of the C-O functional group.

The three samples showed the presence of carbon atoms arranged to form RGO structures, where the C=C bond was sp^2 hybridized [35]. This sp^2 hybridization means the mixing of electrons in 2s orbitals with 2p orbitals, resulting in two 2p orbitals, each containing one electron and one 2pz orbital, which are not hybridized to produce hybridization in three combined orbitals between 2s and 2px, 2py orbitals and one 2pz orbital each that is not hybridized, so that it produces hybridization in three combined orbitals between 2s and 2px, 2py orbitals and one 2pz orbital, each not hybridized. Three hybridized 2p orbitals form a trigonal structure (three angles) that has three carbon atoms with three sp^2 orbitals and one non-hybridized p orbital perpendicular to the sp^2 orbitals. Sp^2 hybridization is the basis of all graphene structures and aromatic compounds. A graphite structure that forms a hexagonal ring is composed of several carbon atoms arranged in parallel between the layers of their fields and bound to three other carbon atoms so that they are included in sp^2 hybridization. Each layer of the graphite structure is a layer of the graphene structure. Two carbon atoms can be joined by sigma bonds formed by the overlap of one sp^2 orbital from each carbon atom. This sigma bond is only one of the bonds of the C=C double bond [35]. Another bond that can form a C=C double bond originates from the p orbitals of each non-hybridized carbon atom that forms a phi bond (π) by overlapping between the sides of the p orbitals of each carbon atom. The phi bond (π) between one hexagonal plane and another plane can be released in the presence of certain energy, but the phi bond between the hexagonal plane layers is not easily broken.

3.1.5 Analysis of UV-Vis Spectroscopy

The optical properties of RGO were obtained from absorbance testing. The absorbance of RGO was scanned spectrophotometrically in the wavelength range of 190 to 500 nm. The wavelength absorbed by RGO is basically influenced by the crystal structure formed in the phase [35]. The results obtained show the behavior after adding PEG to the RGO sample. The high number of reflectance and absorbance peaks (Figures 5 and 6) is probably due to the fact that oxidized RGO has a high absorption of UV radiation [44]. This is also related to the π conjugation in the RGO structure. Graphene oxide has a disrupted π conjugation because there are many oxygen groups and a defect in its structure appears. The reduction in graphene oxide is responsible for the recovery of π conjugation, which is the result of optical absorption by a material [39]. Figure 4 shows that

the pure RGO had strong UV absorption at 250 nm, which can be ascribed to the π - π* transition of the C=C bond. Shoulder peaks are visible at 365 nm, indicating the n-π* transition of the carboxyl groups [37].

RGO is composed of a hexagonal lattice arranged by connecting peaks but has a wide enough distortion to experience a bond defect in the form of a loose carbon bond, which makes it quite difficult to excite the bonded atoms. The difficulty of exciting atoms results in a large energy requirement to break the bonds between them. Therefore RGO absorbs large wavelengths so that energy is needed to release the bonds. The energy gap value in RGO powder is 1.24 eV. Therefore, RGO, which is the constituent sheet of graphite, is also a material that can conduct electric current quite well [29]. The smaller the agglomerating particles (as can be seen in Figure 1), the more grain boundaries occur, so that the bonds between atoms at the grain boundaries increase. The more bonds over the grain, the larger the energy required to remove electrons at the grain boundary. Furthermore, to get the higher energy requires shooting with a short λ. This causes RGO-PEG powder to absorb a reasonably long λ [39].

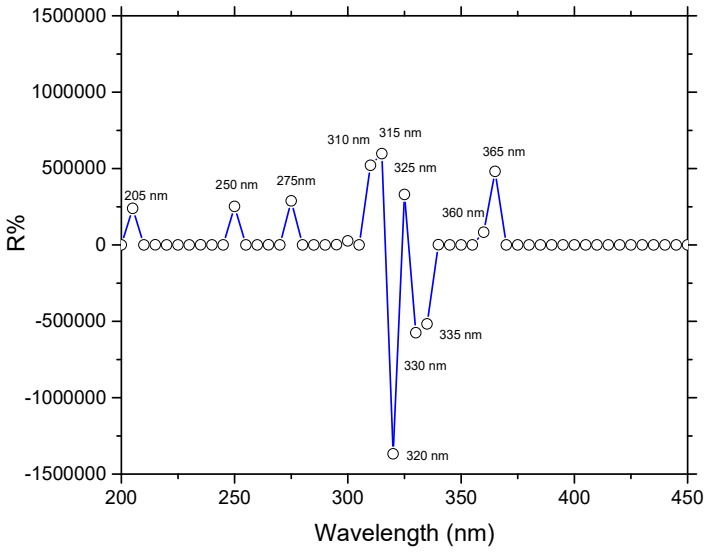

Figure 5 UV-Vis spectra of RGO-PEG powder: reflectance versus wavelength.

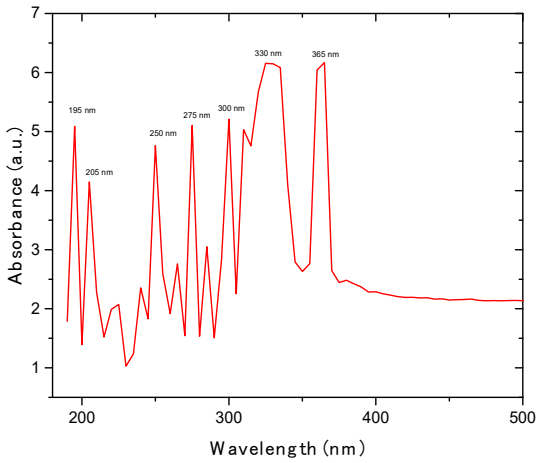

Figure 6 UV-Vis spectra of RGO-PEG: absorbance versus wavelength.

4 Conclusion

It can be concluded that corncob waste has tremendous potential to produce RGO, as evidenced by the presence of C=C and C-C functional groups. The prepared RGO-PEG samples in this work confirm its potency for use as efficient semiconductor material. The characterizations demonstrated that some of the oxygen groups were removed and the sp2 of carbon was recovered during the synthesis process. The most important advantage of corncobs is that they are abundantly available, cost-effective, and the isolation of the product is easy because it can be extracted from plant waste or inedible plant products. The energy gap values and high carbon to oxygen ratio of corncobs were evaluated. Interestingly, the energy gap value was below 2 eV, indicating that the prepared RGO-PEG powder was a semiconductor material. As a final remark, the proposed synthesis approach is a new method to synthesize RGO as a semiconductor material with effective and low-cost production.

Acknowledgment

The authors thank the Ministry of Research, Technology, and Higher Education for funding this research through the research grant scheme (Research in Higher Education Collaboration) with Universitas Negeri Malang (research contract number: 001/LPPM/UNIPDU/PNL/2019).

References

[1] Putra, G.B.A., Pradana, H.Y., Soenaryo, D.E.T., Baqiya, M.A. & Darminto, *Synthesis of Green Fe^{3+}/glucose/rGO electrode for Supercapacitor Application Assisted by Chemical Exfoliation Process from Burning Coconut Shell*, AIP Conf. Proc., **1945**(1), 020040, 2018. DOI: 10.1063/1.5030262.

[2] Khambali, I., Ardiani, I.S., Kurniawan, A.R., Triwikantoro, Zainuri, M. & Darminto, *Synthesis of N-Doped Reduced Graphene Oxide from Coconut Shell as Supercapacitors*, Mater. Sci. Forum, 966 MSF, pp. 437-443, 2019. DOI: 10.4028/www.scientific.net/MSF.966.437.

[3] Xiaolin, Z., Min, W., Jie, L. & Yongfu, L., *Supercapacitors based on High-Surface-Area Graphene,* Nanomaterials, **57**(2), pp. 278-283, 2014.

[4] Lv, M., Yan, L., Liu, C., Su, C., Zhou, Q., Zhang, X., Lan, Y., Zheng, Y., Lai, L., Liu, X. & Ye, Z., *Non-covalent Functionalized Graphene Oxide (GO) Adsorbent with an Organic Gelator for Co-adsorption of Dye, Endocrine-disruptor, Pharmaceutical and Metal Ion*, Chem. Eng. J., **349**, pp. 791-799, 2018, DOI: 10.1016/j.cej.2018.04.153.

[5] Ma, T., Chang, P.R., Zheng, P., Zhao, F. & Ma, X., *Fabrication of Ultra-Light Graphene-based Gels and Their Adsorption of Methylene Blue*, Chem Eng J., **240**, pp. 595-600, 2014.

[6] Feng, L. & Liu, Z., *Graphene in Biomedicine: Opportunities and Challenges,* Nanomedicine, **6**(2), pp. 317-324, 2011.

[7] Mishra, S. & Acharya, R., *Photocatalytic Applications of Graphene Based Semiconductor*, Mater. Today Proc., **35**(2), pp. 164-169, 2021. DOI: 10.1016/j.matpr.2020.04.066.

[8] Masudah, K.W., Yuwita, P.E., Taufiq, A. & Sunaryono, S., *Fabrication of Nanocrystalline Carbon Based on Corncobs Charcoal*, AIP Conf. Proc., **2231**, 040020(April), 2020. DOI: 10.1063/5.0002468

[9] B. Mortazavi, M. E. Madjet, M. Shahrokhi, S. Ahzi, X. Zhuang, & T. Rabczuk, *Nanoporous Graphene: A 2D Semiconductor with Anisotropic Mechanical, Optical and Thermal Conduction Properties*, Carbon N. Y., **147**, pp. 377-384, 2019. DOI: 10.1016/j.carbon.2019.03.018.

[10] Wu, Z.S., Zhou, G., Yin, L.C., Ren, W., Li, F. & Cheng, H.M., *Graphene/Metal Oxide Composite Electrode Materials for Energy Storage*, Nano Energy, **1**(1), pp. 107-131, 2012. DOI: 10.1016/j.nanoen.2011.11.001.

[11] Hasegawa, G., Aoki, M., Kanamori, K., Nakanishi, K., Hanada, T. & Tadanaga, K., *Monolithic Electrode for Electric Double-Layer Capacitors Based on Macro/Meso/Microporous S-containing Activated Carbon with High Surface Area*, J. Mater. Chem., **21**(7), pp. 2060-2063, 2011. DOI: 10.1039/c0jm03793a.

[12] Jain, R., Wadekar, P.H., Khose, R.V., Pethsangave, D.A. & Some S., *MnO_2@Polyaniline-CNT-boron-doped Graphene as a Freestanding Binder-free Electrode Material for Supercapacitor*, J Mater Sci Mater Electron, **31**(11), pp. 8385-8393, 2020.

[13] Liu, C., Yu, Z., Neff, D., Zhamu, A. & Jang, B.Z., *Graphene-based Supercapacitor with an Ultrahigh Energy Density*, Nano Lett., **10**(12), pp. 4863-4868, 2010.

[14] Wadekar, P.H., Ahirrao, D.J., Khose, R.V., Pethsangave, D.A., Jha, N. & Some, S., *Synthesis of Aqueous Dispersible Reduced Graphene Oxide by the Reduction of Graphene Oxide in Presence of Carbonic Acid,* Chemistry Select, **3**(20), pp. 5630-5638, 2018.

[15] Asih, R., Baqiya, M.A., Sari, D.P. & Watanabe, I., *Magnetic Order in Defective Reduced Graphene Oxides (rGO) Investigated using μSR*, **52**, 169, 2019.

[16] Kurniasari, Maulana, A. Nugraheni, A.Y. Jayanti, D.N., Mustofa, S., Baqiya, M.A. & Darminto, *Defect and Magnetic Properties of Reduced Graphene Oxide Prepared from Old Coconut Shell,* IOP Conf Ser Mater Sci Eng Pap., **196**, 012021, pp. 5–9, 2017.

[17] Gao, X., Qu, H., Shan, S., Song, C., Baranenko, D., Li, Y. & Lu, W., *A Novel Polysaccharide Isolated from Ulva Pertusa: Structure and Physicochemical Property*, Carbohydr Polym, **233**, 115849, 2020.

[18] Prasad, C., Liu, Q., Tang, H., Yuvaraja, G., Long, J., Rammohan, A. & Zyryanovc, G.V., *An Overview of Graphene Oxide Supported Semiconductors Based Photocatalysts: Properties, Synthesis and Photocatalytic Applications*, J Mol Liq, **297**, 111826, 2020.

[19] Wang, H., Lai, X., Zhao, W., Chen, Y., Yang, X., Meng, X. & Li, Y., *Efficient Removal of Crystal Violet Dye Using EDTA/ Graphene Oxide Functionalized Corncob: A Novel Low Cost Adsorbent*, **9**(38), pp. 21996-22003, 2019.

[20] Zhao, G., Sun, Y., Zhou, W., Wang, X., Chang, K., Liu, G. Liu, H., Kako, T. & Ye, J., *Superior Photocatalytic H_2 Production with Cocatalytic Co/Ni Species Anchored on Sulfide Semiconductor*, Adv Mater, **29**(40), pp. 1-9, 2017.

[21] Zhao, G., Huang, X., Wang, X. & Wang, X., *Progress in Catalyst Exploration for Heterogeneous CO_2 Reduction and Utilization: A Critical Review*, J Mater Chem A, **5**(41), pp. 21625-21649, 2017.

[22] Huang, K., Yu, H., Xie, M., Liu, S. & Wu, F., *Effects of Poly (Ethylene Glycol)-Grafted Graphene on The Electrical Properties of Poly (Lactic Acid) Nanocomposites*, RSC Adv. **9**(19), pp. 10599-10605, 2019.

[23] Li, Y., Li, Y, Huang, X., Zheng, H., Lu, G., Xi, Z. & Wang, G., *Graphene-CoO/PEG Composite Phase Change Materials with Enhanced Solar-To-Thermal Energy Conversion and Storage Capacity*, Compos Sci Technol, **195**(July), 108197, 2020.

[24] Asmarani, O., Pertiwi, A.D. & Tri Puspaningsih, N.N., *Application of Enzyme Cocktails from Indonesian Isolates to Corncob (Zea Mays) Waste Saccharification*, Biocatal Agric Biotechnol, **24**(February), 101537, 2020.
[25] Piskorski, K., Passi, V., Ruhkopf, J., Lemme, M.C. & Przewlocki, H.M., *Graphene-Insulator-Semiconductor Capacitors as Superior Test Structures for Photoelectric Determination of Semiconductor Devices Band Diagrams*, AIP Adv, **8**(5), 055203, 2018.
[26] Colinge J.-P. & Colinge CA., *Physics of Semiconductor Devices, 1st ed*, New York, Kluwer Academic Publishers, pp. 1-441, 2006.
[27] Taufiq, A., Ikasari, F.N., Yuliantika, D., Sunaryono, S., Mufti, N., Susanto, H., Suarsini, E., Hidayat, N., Fuad, A., Hidayat, A. & Diantoroa, M., *Structural, Magnetic, Optical and Antibacterial Properties of Magnetite Ferrofluids with PEG-20000 Template*, Mater Today Proc., **17**, pp. 1728-1735, 2019.
[28] Zhou, Q., Cai, W., Zhang, Y., Liu, J., Yuan, L., Yu, F., Wang, X. & Liu, M., *Electricity Generation from Corn Cob Char though a Direct Carbon Solid Oxide Fuel Cell*, Biomass and Bioenergy, **91**, pp. 250-258, 2016.
[29] Kazempour, M., Namazi, H., Akbarzadeh, A. & Kabiri, R., *Synthesis and Characterization of PEG-Functionalized Graphene Oxide as an Effective Ph-Sensitive Drug Carrier*, Artif Cells, Nanomedicine Biotechnol, **47**(1), pp. 90-94, 2019.
[30] Upadhyay, S., Bagheri, S. & Abd Hamid, S.B., *Enhanced Photoelectro-chemical Response of Reduced-Graphene Oxide/Zn 1-Xagxo Nanocomposite in Visible-Light Region*, Int J Hydrogen Energy, **39**(21), pp. 11027-11034, 2014.
[31] Hassanien, A.S. & Akl, A.A., *Effect of Se Addition on Optical and Electrical Properties of Chalcogenide Cdsse Thin Films*, Superlattices Microstruct, **89** (January 2019), pp. 153-169, 2016.
[32] Farma, R., Fadilah, R., Awitdrus, A., Sari, N.K., Taer, E., Saktioto, T. & Deraman, M., *Corn Cob Based Activated Carbon Preparation Using Microwave Assisted Potassium Hydroxide Activation for Sea Water Purification*, J Phys Conf Ser., November, **1120**(1), 012017, 2018.
[33] Mas'udah, K.W., Astuti, F. & Darminto, D., *Study on Physical Properties of Reduced Graphene Oxide from Heating Coconut Shell*, JPSE (Journal Phys Sci Eng., **1**(1), pp. 1-6, 2016.
[34] Nugraheni, A.Y., Nashrullah, M. & Prasetya, F.A., *Study on Phase, Molecular Bonding, and Bandgap of Reduced Graphene Oxide Prepared by Heating Coconut Shell*, **827**(1), pp. 285-289, 2015.
[35] Mas'udah, K.W., Diantoro, M. & Fuad, A., *Synthesis and Structural Analysis of Silicon Carbide from Silica Rice Husk and Activated Carbon Using Solid-State Reaction*, J Phys Conf Ser., **1093**(1), pp. 1-6, 2018.

[36] Hayyan, M., Abo-hamad, A., Alsaadi, M.A. & Hashim, M.A., *Functionalization of Graphene Using Deep Eutectic Solvents*, Nanoscale Res Lett., **10**, 324, 2015.

[37] Johra, F.T., Lee, J., Jung, W., *Facile and Safe Graphene Preparation on Solution Based Platform Journal of Industrial and Engineering Chemistry Facile and Safe Graphene Preparation on Solution Based Platform*, J Ind Eng Chem., **20**(5), pp. 2883-2887, 2014.

[38] Zhuo, Q., Gao, J., Peng, M., Bai, L., Deng, J., Xia, Y., Ma, Y., Zhong, J. & Sun, X., *Large-Scale Synthesis of Graphene by the Reduction of Graphene Oxide at Room Temperature Using Metal Nanoparticles as Catalyst*, Carbon N Y, **52**, pp. 559-564, 2012.

[39] Fessenden, R.J. & Gyorgyib, L., *Identifying Functional Groups in IR Spectra Using an Artificial Neural Network*, J Chem Soc Perkin Trans, **2**(1), pp. 1755-1762, 1991.

[40] Nguyen, P.T.N., Salim, C., Kurniawan, W. & Hinode, H., *A Non-Hydrolytic Sol-Gel Synthesis of Reduced Graphene Oxide/TiO_2 Microsphere Photocatalysts*, Catal Today, **230**, pp. 166-173, 2014.

[41] Nugraheni, A.Y., Jayanti, D.N., Kurniasari, Soontaranon, S., Rachman Putra, E.G. & Darminto, *Structural Analysis on Reduced Graphene Oxide Prepared from Old Coconut Shell by Synchrotron X-Ray Scattering*, IOP Conf Ser Mater Sci Eng., **b196**(1), 012007, 2017.

[42] Khalili, D., *Graphene Oxide: A Promising Carbocatalyst for the Regioselective Thiocyanation of Aromatic Amines, Phenols, Anisols and Enolizable Ketones by Hydrogen Peroxide/KSCN in Water,* New J Chem., **40**, pp. 2547-2553, 2016.

[43] Mazurkiewicz-Pawlicka, M., Nowak, M., Malolepszy, A., Witowski, A., Wasik, D., Hu, Y. & Stobinski, L., *Graphene Oxide with Controlled Content of Oxygen Groups as a Filler for Polymer Composites Used for Infrared Radiation Shielding*, Nanomaterials, **10**(1), pp. 8-11, 2020.